# Catalytic Mechanism of NADP$^+$-Dependent Isocitrate Dehydrogenase: Implications from the Structures of Magnesium–Isocitrate and NADP$^+$ Complexes†

James H. Hurley,‡,§ Antony M. Dean,‖ Daniel E. Koshland, Jr.,‖ and Robert M. Stroud*,‡

*Department of Biochemistry and Biophysics and Graduate Group in Biophysics, University of California, San Francisco, California 94143-0448, and Department of Molecular and Cell Biology, University of California, Berkeley, California 94720*

*Received June 7, 1990; Revised Manuscript Received May 31, 1991*

ABSTRACT: The structures of NADP$^+$ and magnesium isocitrate bound to the NADP$^+$-dependent isocitrate dehydrogenase of *Escherichia coli* have been determined and refined at 2.5-Å resolution. NADP$^+$ is bound by the large domain of isocitrate dehydrogenase, a structure that has little similarity to the supersecondary structure of the nucleotide-binding domain of the lactate dehydrogenase-like family of nucleotide-binding proteins. The coenzyme-binding site confirms the fundamentally different evolution of the isocitrate dehydrogenase-like and the lactate dehydrogenase-like classes of nucleotide-binding proteins. In the magnesium–isocitrate complex, magnesium is coordinated to the $\alpha$-carboxylate and $\alpha$-hydroxyl oxygen of isocitrate in a manner suitable for stabilization of a negative charge on the hydroxyl oxygen during both the dehydrogenation and decarboxylation steps of the conversion of isocitrate to $\alpha$-ketoglutarate. The metal ion is also coordinated by aspartate side chains 283′ (of the second subunit of the dimer) and 307 and two water molecules in a roughly octahedral arrangement. On the basis of the geometry of the active site, the base functioning in the dehydrogenation step is most likely aspartate 283′. *E. coli* isocitrate dehydrogenase transfers a hydride stereospecifically to the A-side of NADP$^+$, and models for a reactive ternary complex consistent with this stereospecificity are discussed.

Isocitrate dehydrogenase is a key enzyme of the Krebs cycle and, as such, appears in species from man to bacteria. This range makes its structure of great interest, but the isocitrate dehydrogenase (IDH)[1] of *Escherichia coli* represents a new class of enzymes regulated by phosphorylation at the active site (Hurley et al., 1990; Dean & Koshland, 1990). Thus, not only its structure but its regulation and kinetic characteristics become relevant to evolutionary and functional considerations.

IDH [D$_s$-*threo*-isocitrate-NAD(P)$^+$ oxidoreductase (decarboxylating), E.C. 1.1.1.42] also belongs to a class of metal-ion-dependent decarboxylating dehydrogenases that includes the homologous isopropylmalate dehydrogenase (IMDH) (Thorsness & Koshland, 1987) and the L-malate enzyme, which has an unrelated sequence (Bagchi et al., 1987; Kobayashi et al., 1989). Each of these enzymes has a structurally similar substrate, HOOC(HO)CHCH(X)COOH, in which X represents the $CH_2$(COOH) of isocitrate, the $CH(CH_3)_2$ of isopropylmalate, and the hydrogen of malate. Each catalyzes a chemically equivalent reaction: dehydrogenation at the $\alpha$-carbon to form a carbonyl group from a hydroxyl group; and decarboxylation at the $\beta$-carbon.

Despite a lack of sequence similarity, the nucleotide-binding domains of many dehydrogenases have remarkably similar structures (Rossmann et al., 1974). This domain, known as the lactate dehydrogenase (LDH) fold after the first enzyme in which it was described (Adams et al., 1970), consists of two $\beta\alpha\beta\alpha\beta$ motifs, each with the $\beta$-strands arranged in parallel and linked by parallel helices. Many other proteins, either nucleotide-binding or with other functions, have topologically similar folds (Richardson, 1981). Although no obvious LDH fold is seen in IDH, a domain with an $\alpha/\beta$ supersecondary structure is present (Hurley et al., 1989, 1990). Despite a topology markedly different from that of the LDH fold, NADP$^+$ might conceivably bind near the N-termini of one or more helices in a manner analogous to NAD$^+$ binding to LDH. However, the $\alpha/\beta$ domain is involved in intersubunit packing in IDH, and this would prevent NADP$^+$ binding unless a conformational change opens up a binding site near the N-termini of the parallel helices. Alternatively, the nucleotide might bind in the interdomain cleft.

The X-ray crystallographic structures of *E. coli* IDH, with and without isocitrate bound, are the first to have been determined in this class of decarboxylating dehydrogenases (Hurley et al., 1989, 1990). As such, they provide the first opportunity for a structural interpretation of the kinetic and physical–chemical studies of the mechanism common to these enzymes. In this study, the binding of NADP$^+$, the role of $Mg^{2+}$ in the catalytic mechanism, and the stereochemistry of the reaction are explored.

## Experimental Procedures

*X-ray Structure Determination.* IDH crystals (Hurley et al., 1989) were presoaked for at least 3 h in a freshly prepared solution of 300 mM $\beta$-NADP$^+$ (sodium salt, Sigma), 100 mM NaCl, 35 mM $Na_2HPO_4$, 2 mM DTT, and 0.02% $NaN_3$ in 45% saturated $(NH_4)_2SO_4$, with the pH adjusted to 6.0 with

† This work was supported by the National Institutes of Health Grant GM 24485 to R.M.S. and the National Science Foundation Grant 04200 and Markey Charitable Trust support to D.E.K., Pittsburgh Supercomputer Center Grant DMB 890040P to R.M.S. for crystallographic refinement, and a University of California Regent's Fellowship to J.H.H. Atomic coordinates of the magnesium–isocitrate and NADP$^+$ complexes with isocitrate dehydrogenase have been deposited with the Brookhaven Protein Data Bank.

* To whom correspondence should be addressed.

‡ University of California, San Francisco.

§ Present address: Institute of Molecular Biology, University of Oregon, Eugene, OR 97403.

‖ University of California, Berkeley.

[1] Abbreviations: IDH, isocitrate dehydrogenase; IMDH, 3-isopropylmalate dehydrogenase; LDH, lactate dehydrogenase; NOE, nuclear Overhauser effect; prr, proton relaxation rates.

0006-2960/91/0430-8671$02.50/0 

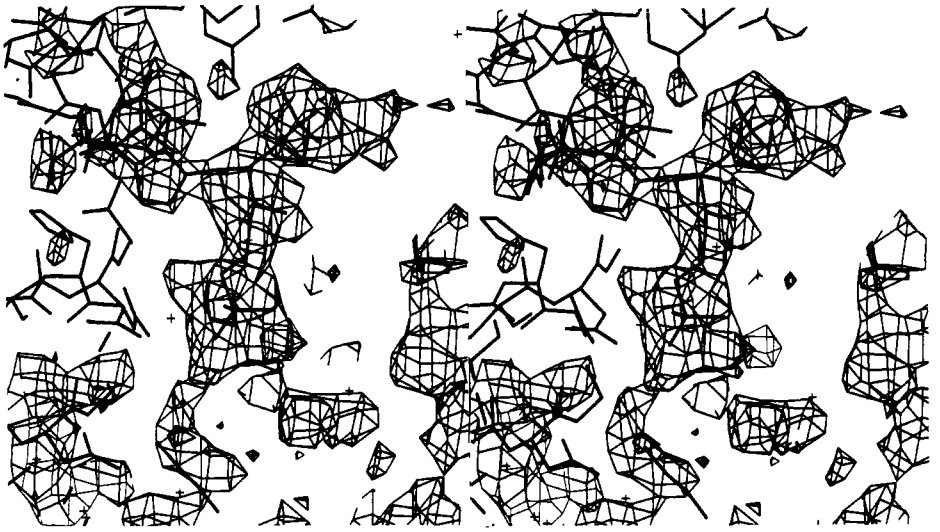

FIGURE 1: Refined structure of the well-ordered fragment of $NADP^+$ in positive difference electron density from a $(F_o - F_c)\alpha_{calc}$ synthesis at 2.5-Å resolution with $F_c$ and phases calculated from the unliganded structure of IDH after removal of all solvent molecules. The difference electron density is contoured at 3 standard deviations. The difference density at lower left, the largest feature in the map excepting $NADP^+$, corresponds to solvent molecule 417 and is also present in unliganded IDH.

Table I: Crystallographic Statistics for the $NADP^+$ Complex with IDH[a]

| | | | | | | |
|---|---|---|---|---|---|---|
| max resolution | 4.5 | 3.6 | 3.1 | 2.85 | 2.65 | 2.49 |
| $R_{merge}$ | 0.059 | 0.090 | 0.157 | 0.246 | 0.342 | 0.43 |
| $\langle I\rangle/\sigma\langle I\rangle$ | 68.9 | 35.1 | 15.2 | 7.0 | 3.8 | 2.1 |

[a] Cell parameters are $a = b = 105.1$ Å and $c = 150.3$. The space group is $P4_32_12$. $R_{merge} = \sum|Ii - \langle I\rangle|/\sum\langle I\rangle$, where the summation is over all observations from three crystals. $\langle I\rangle/\sigma\langle I\rangle$ is the mean ratio of average intensities over the standard deviation of the average intensity. The statistics shown are for shells to reciprocal shape.

concentrated $NH_4OH$. It had been previously observed that 3 h were sufficient for crystals soaked in NADPH solutions to become colored. X-ray reflection data were collected for three crystals at room temperature with a Nicolet area detector using a CuK$\alpha$ rotating anode X-ray source and reduced with the XENGEN data reduction package (Howard et al., 1987). These crystals were isomorphous with those of the unliganded enzyme. The unweighted merging $R$ factor on intensity for 141 100 observations of 29 217 unique reflections to 2.5-Å resolution was 0.115 (Table I). 96.5% of the possible unique reflections were measured. Density from a 2.5-Å resolution $[F_o(NADP) - F_c(free)]\alpha_{calc}$ difference map (Figure 1) with phases calculated from the refined structure of unliganded IDH allowed unambiguous location of a portion of the NADP molecule corresponding to adenosine 2′,5′-diphosphate. All solvent molecules were removed from the unliganded structure prior to calculation of the difference map. The portion of NADP corresponding to nicotinamide mononucleotide (NMN) could not be located in difference density. Local scaling was used for all map calculations. The model was built with FRODO (Jones, 1985) starting from the small molecule X-ray structure of Li-$NAD^+$ (Saenger et al., 1977). This model was refined with XPLOR minimization (Brunger et al., 1987) to an $R$ factor of 0.181 for 22 342 nonzero reflections from 5.0- to 2.5-Å resolution. No bulk solvent model was included in the refinement. In order to maintain acceptable planarity of the adenine ring, ring-spanning dihedral energy coefficients in the CHARMM nucleic acid parameter library version 11 (Brooks et al., 1983) were increased by a factor of 40, and purine ring improper torsion angle energy coefficients were all increased to 250 kcal. The current model contains 102 water molecules. Bond lengths and angles deviate from target values by 0.016 Å rms and 3.06° rms, respectively. The structure determination for the Mg–isocitrate complex has been described previously (Hurley et al., 1990).

Table II: Possible Hydrogen Bonds and Salt Bridges in the $Mg^{2+}$–Isocitrate Complex[a]

| | | | |
|---|---|---|---|
| O1, Arg 119 NH1 | 3.00 | O6, Tyr 160 OH | 2.80 |
| O1, Arg 129 NH1 | 3.01 | O6, Lys 230′ NZ | 2.96 |
| O2, Arg 129 NH1 | 3.06 | O7, water 560 | 3.00 |
| O2, Arg 153 NH2 | 2.92 | O7, water 562 | 2.78 |
| O2, water 458 | 3.04 | O7, Mg | 1.92 |
| O2, Mg | 2.24 | O7, Asp 283′ OD2 | 2.69 |
| | | O7, Asp 307 OD2 | 2.92 |
| O4, Ser 113 Og | 2.65 | | |
| O4, Asn 115 ND | 3.41 | Mg, Asp 283′ OD2 | 2.34 |
| O5, Arg 119 NH2 | 2.81 | Mg, Asp 307 OD2 | 2.09 |
| O5, Arg 153 NH1 | 3.01 | Mg, water 458 | 2.07 |
| | | Mg, water 562 | 1.86 |

[a] Distances of less than 3.5 Å between potential hydrogen-bond or salt-bridge-forming partners of isocitrate, magnesium, and IDH.

*Stereospecificity.* The stereospecificity of the reaction was studied by adding 30 mg of purified *E. coli* isocitrate dehydrogenase to 1 mL of 5 mM 2*R*,3*S*-isocitrate and 30 $\mu$M [4-$^3$H]NAD (3 Ci/mmol) in 25 mM MOPS, 100 mM NaCl, and 5 mM $MgCl_2$, pH 7.5, in the presence of either 1 mg/mL of L-glutamate dehydrogenase and 5 mM ammonium chloride or 1 mg/mL of L-lactic dehydrogenase and 5 mM pyruvate. After 2 h at 25 °C, 250-mL samples were loaded onto a Waters $C_{18}$ reverse-phase column (3.9 mm by 30 cm) and isocratically eluted with a mobile phase of 5% acetonitrile in 0.05 M phosphoric acid, pH 3.5 at 25 °C, and a flow rate of 1 mL/min. Peak fractions were detected at 214 nm with an on-line UV detector and the counts/peak determined. Peaks were identified by correlating the elution patterns with those obtained by using pure standards.

## RESULTS

*Isocitrate-Binding Site.* $Mg^{2+}$-isocitrate binds in the pocket between the large and small domains of IDH (Figures 2, 3, and 4), and comparisons with the structure of IDH in the absence of $Mg^{2+}$-isocitrate reveal that structural changes are localized to the binding site (Hurley et al., 1990). Hydrogen bonds are formed between isocitrate and serine 113, arginines 119, 129, and 153, tyrosine 160, lysine 230′ (where the prime denotes the second subunit), and five water molecules (Table II). Two of the waters (458 and 479) are present in the

FIGURE 2: Structures of $NADP^+$ and isocitrate bound to IDH, superimposed on an $\alpha$-carbon backbone drawing of the IDH monomer. Substrate and cofactor are seen above the "clasp" loop at the base.

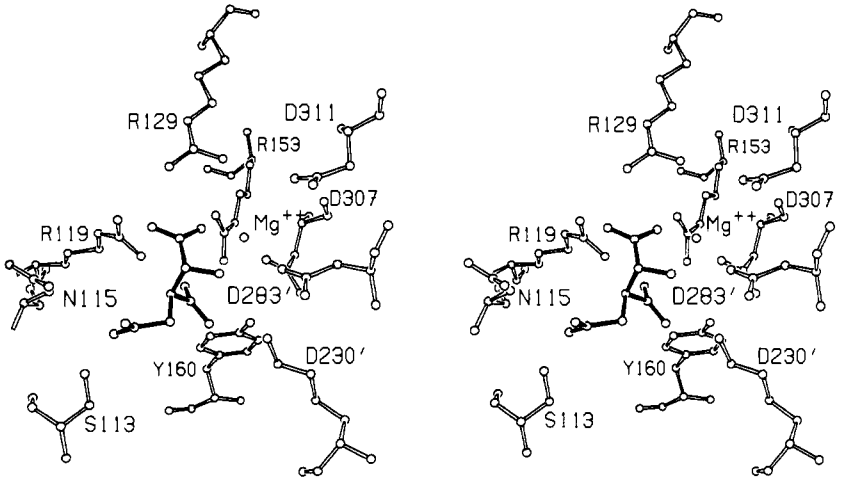


FIGURE 3: Divergent stereoview of the refined structure of the $Mg^{2+}$–isocitrate complex showing the isocitrate-binding site. Both subunits are shown, with labeled residues belonging to the second subunit indicated by a primed number. Waters are not shown. Isocitrate is drawn with solid bonds and the enzyme with open bonds.

unliganded structure of IDH. Three waters (560–562) are unique to the substrate-bound structure. Asparagine 115, with an Nδ–O4 distance of 3.4 Å, may interact electrostatically with isocitrate but probably does not form a hydrogen bond. The C1–C2–C3–C4 and C2–C3–C4–C5 torsion angles of bound isocitrate are −165° and 107°. This brings the γ-carboxylate closer to the α-carboxylate than seen in the small molecule structure of the potassium isocitrate (van der Helm et al., 1968), with torsion angles of −166° and 150°.

A difference map calculated between amplitudes for crystals soaked in $Mn^{2+}$ and $Mg^{2+}$ and isocitrate (Hurley et al., 1990) provides a view of the metal coordination more accurate than would normally be possible at 2.5-Å resolution. The crystal structure shows that the active site $Mg^{2+}$ is coordinated to six oxygen ligands, confirming the conclusions drawn from multinuclear NMR spectra for pig heart enzyme in the presence of $^{113}Cd$–isocitrate (Ehrlich & Colman, 1989) and in a roughly octahedral arrangement (Figure 5). Two ligands are provided by the bidentate chelation of the metal by the O2 of the α-carboxylate and hydroxyl oxygen of isocitrate. This is consistent with the proton relaxation studies of $Mn^{2+}$-isocitrate in free solution (Villafranca & Colman, 1974). Two more ligands are provided by water molecules 458 and 562. Water 458 is present in the unliganded structure, but water 562 is unique to the substrate-bound structure. The presence of only one metal-bound water molecule in the pig heart enzyme–substrate complex was deduced from temperature and frequency dependence of proton relaxation rates (prr) (Villafranca & Colman, 1974). The observation of two metal-bound water molecules in the crystal structure may reflect a difference either in the structure of the active sites

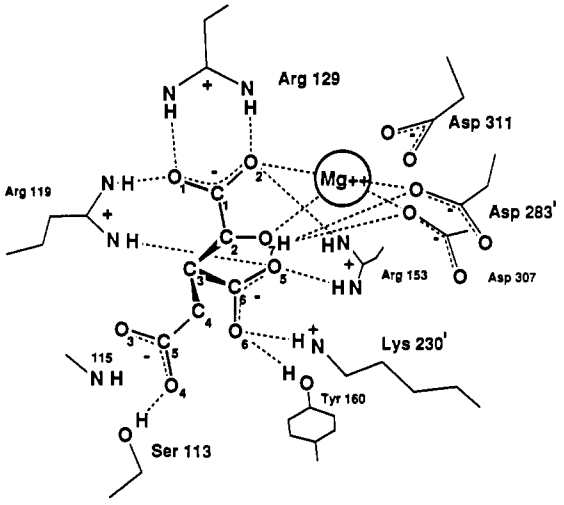


FIGURE 4: Schematic representation of $Mg^{2+}$ and isocitrate bound to IDH [after Hurley et al. (1990)]. A prime indicates residues of the second subunit. Hydrogens believed to be involved in hydrogen bonds to isocitrate are shown for illustrative purposes. Dashed lines indicate likely hydrogen bonds.

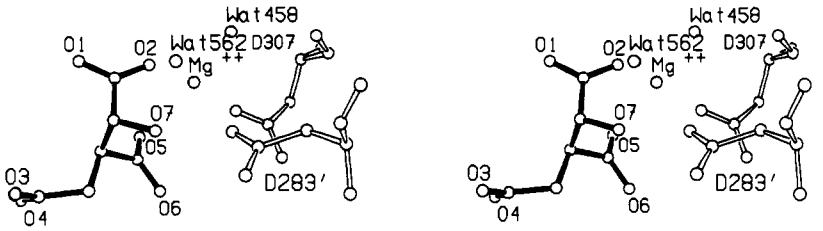


FIGURE 5: Divergent stereoview of the refined structure of the $Mg^{2+}$–isocitrate complex, showing the roughly octahedral coordination of the metal ion by substrate, bound water molecules, and aspartates 283′ and 307. Isocitrate is drawn with solid bonds and the enzyme with open bonds.

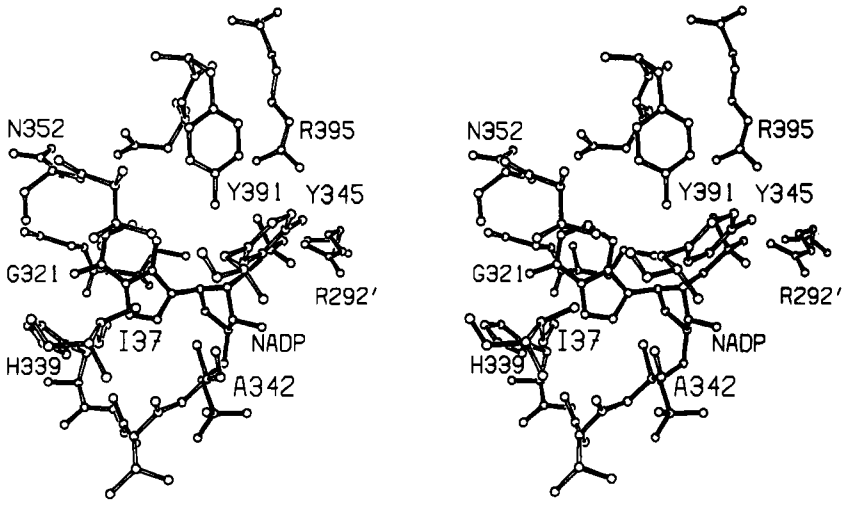


FIGURE 6: Divergent stereoview of the refined structure of the $NADP^+$ complex, showing the environment of the ordered fragment of $NADP^+$ bound to IDH. $NADP^+$ is drawn with solid bonds and the enzyme with open bonds.

of the bacterial and mammalian enzymes or in the presence of a second water with a relaxation time outside the range of the prr experiment. The last two ligands are provided by the side chains of aspartates 283′ and 307 with aspartate 311 as a second-nearest neighbor, 3.5 Å from the metal. The $Mg^{2+}$ is relatively well-ordered, with $B$ = 27 Å$^2$, compared to an average $B$ factor of 29.6 Å$^2$ for the entire structure. The two $Mg^{2+}$-bound water molecules (458 and 562) are also tightly bound, with $B$ factors of 24 and 28 Å$^2$, respectively.

*$NADP^+$-Binding Site.* $NADP^+$ binds in the same cleft as isocitrate, between the large and small domains of the enzyme, and above isocitrate in the views shown in Figures 2 and 3. Only the moieties corresponding to adenosine 2′,5′-diphosphate could be reliably located in electron density (Figure 6). The side chains of isoleucine 37, isoleucine 320, histidine 339, alanine 342, and valine 351, the aliphatic portion of the side chains asparagine 352 and aspartate 392, and the main chain at residues glycine 321 and asparagine 352 form the binding site for the adenine moiety. These residues are identical or conservative substitutions in IMDH. The only obvious hydrogen bond between IDH and the adenine moiety is made between N6 of adenine and the main-chain carbonyl oxygen of residue 352. Although distances as short as 3.07 Å are observed between histidine 339 and N6, the geometry of the present structure would require a hydrogen bond almost normal to the plane of the imidazole ring. This may be a result of the low pH of the soaking conditions necessary for crystal stability, at which the histidine may become protonated. Other potential hydrogen bonds shown in Table III either are longer than typical or have nonideal hydrogen-bond angles.

The adenine ring binds in the anti conformation with respect to the ribose. The observation of an NOE between adenine proton H8 and ribose proton H1′ has led to the suggestion that nucleotides bind to pig heart $NADP^+$-dependent IDH with the adenine–ribose bond in the syn conformation (Ehrlich & Colman, 1985). The H8–H1′ distance is not highly sensitive to the conformation of the adenine–ribose bond, so whether there is a real difference in adenine binding to the *E. coli* and pig heart enzymes remains unclear.

Table III: Possible Hydrogen Bonds and Salt Bridges in the $NADP^+$ Complex[a]

| Adenine | | 2′-Phosphate | |
|---|---|---|---|
| N1, Asp 352 N | 3.22 | O31, Arg 292′ NH2 | 2.92 |
| N3, Tyr 391 OH | 3.45 | O32, Tyr 345 OH | 2.95 |
| N6, His 339 NE2 | 3.07 | O33, Tyr 391 OH | 2.59 |
| N6, Asp 352 O | 3.11 | O33, Arg 395 NH1 | 3.18 |
| N7, His 339 ND1 | 3.31 | | |
| | | 5′-Phosphate | |
| | | O12, Ala 342 N | 2.95 |

[a] Distances of less than 3.5 Å between potential hydrogen-bond or salt-bridge-forming partners of $NADP^+$ and IDH.

Arginines 292′ and 395 and tyrosines 345 and 391 interact with the 2′-phosphate of $NADP^+$ (Table III). The 5′-phosphate group interacts with the main chain from residues 340 to 342, although the position of this moiety is poorly defined. No interactions are found between the enzyme and the adenosine ribose, which is built in the C3′ endo conformation in the present model. The relative lack of protein cofactor interactions and the low level of sequence conservation in part of the cofactor-binding site may reflect the low-affinity binding ($K_d$ = 125 μM; Dean et al., 1989) of the cofactor relative to the potentially large binding energy achievable for a molecule the size of $NADP^+$, as well as the differing cofactor specificity of IDH and IMDH.

Refined $B$ factors for the locatable portion of $NADP^+$ with occupancy fixed at 1.0 range from 31 to 47 Å$^2$ for the adenine moiety, 49 to 65 Å$^2$ for the adenine-linked ribose moiety, 68 to 73 Å$^2$ for the 5′-phosphate; and 50 to 60 Å$^2$ for the 2′-phosphate. The average protein $B$ factor in the $NADP^+$ complex is 28 Å$^2$. Comparison with the structures of IDH in

Table IV: Tritium Transfer from the C4 of NAD+[a]

| elution time | peak identity | total cpms per peak | %cpms per peak |
|---|---|---|---|
| | NAD Alone | | |
| 5 | unknown | 6267 | 1.6 |
| 13 | NAD | 349000 | 89.6 |
| | | | total 91.2 |
| | Glutamate Dehydrogenase Reaction | | |
| 4 | glutamate | 672913.5 | 84.1 |
| 5 | isocitrate | 101507 | 12.6 |
| 13 | NAD | 9068 | 1.2 |
| | | | total 97.9 |
| | Lactate Dehydrogenase Reaction | | |
| 5 | pyruvate | 34069.5 | 2.7 |
| 5 | isocitrate | | |
| 5.5 | lactate | 852 | 0.1 |
| 13 | NAD | 1247288 | 96.0 |
| | | | total 98.8 |

[a] Stereospecific hydride transfer by IDH. Note that the tritium detected in the isocitrate peak when the reaction is coupled to L-glutamate dehydrogenase is the result of some overlap with the glutamate peak.

the absence of $NADP^+$ reveals that structural changes are confined to the immediate vicinity of the active site. The largest shifts are for the two arginine side chains that bind the 2′-phosphate group. NH1 and NH2 of arginine 292 move 1.16 and 1.49 Å, respectively, and NH1 and NH2 of arginine 395 move 2.46 and 1.81 Å, respectively. No other groups in the $NADP^+$-binding site move by more than 1.0 Å, and the rms shift for all protein atoms from the unliganded enzyme is 0.23 Å.

*Stereospecificity.* The stereospecificity of the IDH reaction was examined by coupling it to the reactions of lactate dehydrogenase (LDH) (known to be A stereospecific) and L-glutamate dehydrogenase (known to be B stereospecific). In the experiment, tritium-labeled $NAD^+$ was treated with unlabeled substrates. If IDH places a hydride in the A-position at the C4 of the nicotinamide ring, LDH will remove it and NAD(H) will remain labeled. On the other hand, if IDH places a hydride in the B-position, LDH will remove the tritium to pyruvate, forming labeled lactate. Since tritium is not removed from NAD during the coupled reaction with LDH (Table IV), the hydride transferred by IDH to NAD must be identical with the one removed by LDH to lactate. The trivial explanation that LDH is not active under the assay conditions was eliminated by conducting an experiment in the absence of IDH and monitoring the drop in absorbance at 340 nm of exogenously added NADH.

B-specific dehydrogenases will remove the hydride from the face opposite to that to which IDH adds its hydride. If the IDH reaction is coupled to that of a B-specific dehydrogenase, tritium should be moved from NAD to the final product. As predicted, tritium is moved from the NAD peak to the glutamate peak by the B-specific L-glutamate dehydrogenase (Table IV). This demonstrates that the IDH of *E. coli* has the same stereospecificity as the mammalian enzyme, which is also an A-specific dehydrogenase (Nakamoto & Vennesland, 1960).

## Discussion

*Catalysis.* The oxidation of isocitrate by IDH is believed to occur in two steps (Figure 7). In the first, isocitrate is oxidized to oxalosuccinate (Siebert et al., 1957) by the removal of a proton from the hydroxyl oxygen to a base and the transfer of a hydride to $NADP^+$. The base may well be aspartate 283′. Not only is it the closest potential base to the α-hydroxyl

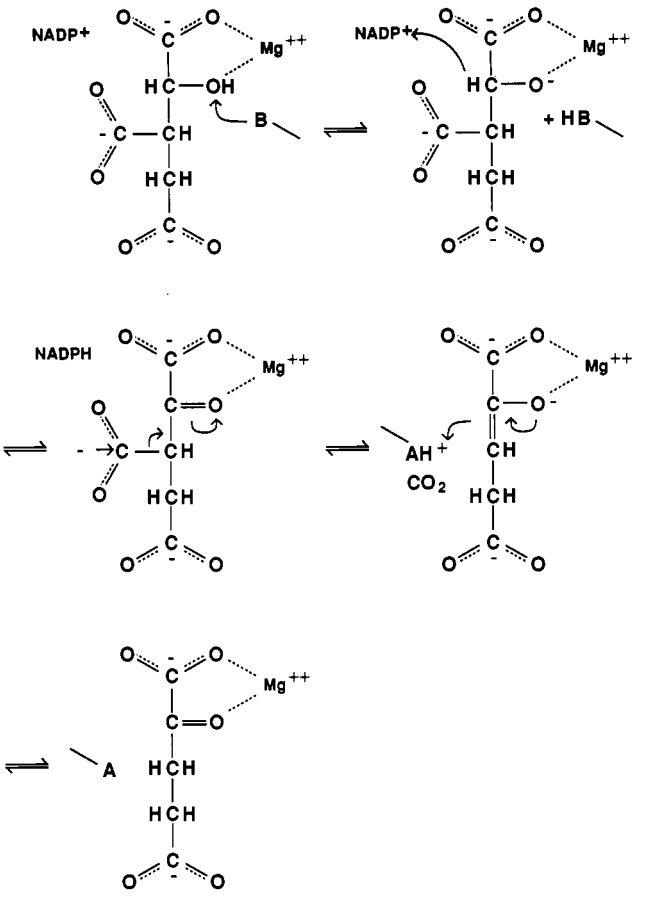


FIGURE 7: Likely mechanism for the reaction catalyzed by IDH. B is probably aspartate 283′, and A is probably either tyrosine 160 or lysine 230′. The second step shows one possibility for the transition state in the dehydrogenation reaction, a fully ionized alcoholate. This transition state would experience the greatest electrostatic stabilization by a metal ion. An alternative, not shown, is concerted transfer of the proton and hydride, in which only a partial negative charge develops on the incipient keto oxygen.

oxygen at 2.6 Å but it appears to be in a particularly favorable geometry for proton transfer. When the hydroxyl proton points directly away from $Mg^{2+}$, protonation of aspartate 283′ would be syn, which has been estimated to be up to $10^4$ times more favorable than anti protonation (Gandour, 1981).

In the second step of the reaction, the β-carboxylate of oxalosuccinate is lost as $CO_2$ (Londesborough & Dalziel, 1968), which is followed by the stereospecific protonation of the β-carbon to form α-ketoglutarate (Lienhard & Rose, 1964). IMDH also catalyzes the stereospecific protonation of the β-hydrogen with the same retention of configuration as IDH (Kakinuma et al., 1989). This suggests that residues common to both enzymes may be involved. Tyrosine 160 and lysine 230′ are identical in both enzymes. In IDH they are hydrogen-bonded to the β-carboxylate of isocitrate where they are favorably positioned to serve as the acid catalyst that protonates C3 after decarboxylation. However, this conclusion is tentative because the α-ketoglutarate may bring the C3 closer to some currently unidentified proton donor if α-ketoglutarate has a substantially different mode of binding from isocitrate.

The X-ray crystal structure shows a $Mg^{2+}$ ion coordinated by the oxygens of the α-carboxylate and C2 hydroxyl of isocitrate. This $Mg^{2+}$ is in a position to stabilize the negative charge formed on the hydroxyl oxygen during dehydrogenation. Such electrostatic stabilization of the transition state is a common feature of dehydrogenases, provided by arginine 109 in lactate dehydrogenase (Clarke et al., 1986) and $Zn^{2+}$

in alcohol dehydrogenase (Branden et al., 1975).

The $Mg^{2+}$-dependent enzymatic $\beta$-decarboxylation of $\alpha$-ketoacids is thought to be similar to the $Mg^{2+}$-catalyzed reaction in solution, where the metal ion is believed to be coordinated by the keto oxygen and the adjacent $\alpha$-carboxylate and stabilizes the formation of an enolate intermediate (Steinberger & Westheimer, 1951). It should be noted that decarboxylation proceeds from oxalosuccinate rather than from isocitrate. These compounds are not isosteric because oxalosuccinate and the presumed enolate transition state are planar at the $\alpha$-carbon, whereas isocitrate is tetrahedral. Nevertheless, the amino acid residues involved in binding and the general features of metal coordination for isocitrate, oxalosuccinate, and the transition state are probably similar.

The finding of the $Mg^{2+}$ ion in precisely the position needed to catalyze the reaction via the Steinberger and Westheimer mechanism is an excellent confirmation of those concepts. Moreover, $^{13}C$ NMR resonances characteristic of the enol form of enzyme-bound $\alpha$-ketoglutarate have been observed (Ehrlich & Colman, 1987). Thus, $Mg^{2+}$ appears to play the central role in transition-state stabilization for both steps in the IDH reaction, as shown in Figure 7.

The $^{13}C$ isotope effect for the decarboxylation of oxalosuccinate by pig heart IDH is barely measurable (Grissom & Cleland, 1988), suggesting a large acceleration in rate for this step. The similar malic enzyme accelerates the decarboxylation of oxaloacetate by roughly a factor of $10^8$ (Seltzer et al., 1959). Presumably, solvent exclusion in the active site cleft produces a large increase in the electrostatic stabilization of the proposed enolate intermediate by the $Mg^{2+}$ ion. This enhances the transfer of the negative charge from the $\beta$-carboxylate of oxalosuccinate to the enolate oxygen over a distance of 3.4 Å, and hence accelerates decarboxylation. The small divalent magnesium ion might provide a sufficiently potent electrostatic field at the carbonyl oxygen that an electron can be moved from the $\beta$-carboxylate despite the strong salt bridge and the hydrogen-bond interactions between this group and arginines 119 and 153, tyrosine 160, and lysine 230′. The positive charges at these residues may provide enough binding energy to desolvate trianionic isocitrate, even at the expense of some destabilization of the transition state. Another key feature of the transition state is the change in hybridization at C3 ($sp^3$ to $sp^2$). There is no indication of strain that might favor a trigonal over a tetrahedral geometry at C3, although this might not be fully evident at 2.5-Å resolution.

*Substrate Specificity of IDH and Related Enzymes.* Sequence comparison with IMDH reveals a consistent picture of the evolution of substrate specificity for the IDH-like class of decarboxylating dehydrogenases. All residues (119, 129, 153, 160, and 230′) interacting with the $\alpha$- and $\beta$-carboxylates and $\alpha$-hydroxyl moieties of isocitrate, which are common to isocitrate, isopropylmalate, and malate, are conserved between IDH and all known IMDH sequences. The two aspartates, 283′ and 307, coordinating $Mg^{2+}$ are also conserved in all available sequences. Aspartate 311, a second-nearest neighbor to the metal, is conserved in all sequences except that of the extreme thermophile *Thermus thermophilus* (Kagawa et al., 1984), in which it is replaced by asparagine. Residues interacting with the $\gamma$-carboxylate of isocitrate, 113 and 115, are unique to isocitrate and are not conserved with the IMDH sequences. The common features of IDH and IMDH are thus due to conserved residues interacting with the $\alpha$- and $\beta$-groups and the metal ion, with differing substrate specificity determined by nonconserved residues interacting with the $\gamma$-group. There is no homology with the L-malic enzyme sequence

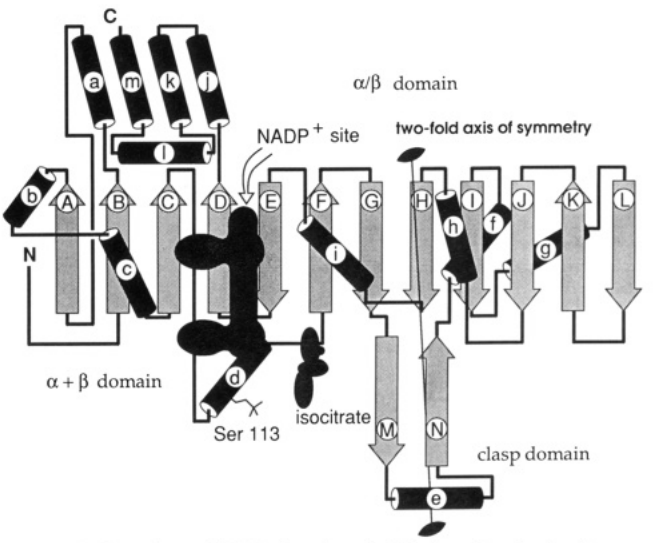


FIGURE 8: Topology of IDH showing the binding sites for isocitrate and NADP in reference to the overall fold. Ser 113 phosphate is located in helix d. The 2-fold symmetry axis that relates monomers in the dimer is indicated.

(Bagchi et al., 1987; Kobayashi et al., 1989), which is expected given the opposite stereospecificities of the two enzymes. It is likely that homologies will be found with the D-malic enzymes, yet to be sequenced. Given the topological dissimilarity of IDH to previously characterized dehydrogenases (Hurley et al., 1989), the metal-dependent decarboxylating *R*-hydroxyacid dehydrogenases appear to form a family evolutionarily distinct from other dehydrogenases.

*Unique Nucleotide-Binding Fold of IDH.* $NADP^+$ binds in the interdomain cleft (Figure 8), rather than at the N-termini of the parallel helices in the $\alpha/\beta$ supersecondary structures in the small domain that mimic the LDH fold (Figure 8). The pyrophosphate moiety of $NADP^+$ binds near the N-terminus of the helical turn formed by residues 342–346 in IDH, and hydrogen bonds may form with the peptide nitrogens of residues 340–342. In this one respect, the binding of $NADP^+$ to IDH is analogous to the many LDH-like folds that exploit the partial positive charges at the N-termini of parallel $\alpha$-helices in binding the negatively charged phosphate moieties of the nucleotide (Wierenga et al., 1985).

A growing number of instances of unconventional nucleotide-binding folds are appearing, demonstrating multiple evolutionary solutions to a common biological problem. Medium chain acyl-CoA dehydrogenase (Kim & Wu, 1988), 6-phosphogluconate dehydrogenase (Adams et al., 1986), beef liver catalase (Fita & Rossmann, 1985), and IDH bind nucleotides in folds that are distinct from that of LDH. None of these folds is topologically similar. The structurally distinct $NADP^+$-binding site of IDH supports the notion that the evolution of the decarboxylating dehydrogenases is distinct from that of most other dehydrogenases.

The amino acids involved with nucleotide binding are not as well conserved as those binding the substrates. The substitutions for residues interacting with the 2′-phosphate of $NADP^+$ may well account for the different in cofactor specificity between IDH and IMDH, an NAD specific enzyme. Indeed, the substitution of a similar set of residues interacting with the 2′-phosphate of $NADP^+$ bound to glutathione reductase changes this enzyme into an $NAD^+$-specific dehydrogenase (Scrutton et al., 1990).

McKee et al. (1989) have suggested on the basis of circular dichroism (CD) difference spectra from 260 to 280 nm that *E. coli* IDH undergoes a conformational change on binding $NADP^+$. We have found minimal conformational changes in

the crystallographic structure of $NADP^+$ bound to IDH, with no observable change in environment of any tryptophan residue. Given that both domains of IDH are constructed on the rigid framework of a common $\beta$-sheet, it seems unlikely that any conformational change exists along the reaction pathway of IDH that brings the small domain into contact with the cofactor. Although there may be some question about the units used in Figure 1 by McKee et al. (1989), the small changes in the near-UV CD spectrum of IDH on cofactor binding are apparently of a magnitude accountable for by the electrostatic effect of the 2'-phosphate on tyrosines 345 and 391, by binding the adenine ring of $NADP^+$ to the enzyme, or both. This hypothesis makes consistent the present observations and those of McKee et al. (1989).

Comparison of the conformation of $NADP^+$ bound to IDH with the conformation of $NAD(P)^+$ bound to other dehydrogenases is not possible because the NMN portion of $NADP^+$ could not be located. $NADP^+$ is stable at pH 6.0 (Oppenheimer, 1987); therefore it is unlikely that the nicotinamide moiety has been cleaved during 5 days of data collection. Mas and Colman (1985) have reported substantial inhibition of nucleotide binding to pig heart $NADP^+$-dependent IDH by 0.15 M sulfate. It is likely either that the NMN moiety is disordered in the binary complex of $NADP^+$ with isocitrate or that this moiety is disordered under the very high sulfate and low pH conditions in which IDH crystals are stable.

There is unambiguous evidence from measurements of NOEs between nicotinamide and ribose protons of $NAD^+$ in the absence of isocitrate that the nicotinamide–ribose bond is in the anti conformation (Ehrlich & Colman, 1985). Because the pig heart and *E. coli* enzymes are both A-side specific, and the nicotinamide–ribose bond is anti in all known cases for A-side specific dehydrogenases, it is reasonable to expect that the conformation will be anti for the *E. coli* enzyme as well.

The observed structures of magnesium isocitrate and $NADP^+$ bound to *E. coli* IDH and the known A-side specificity of $NADP^+$-dependent IDH's allow speculation on possible structures for the reactive $NADP^+$–magnesium–isocitrate complex. The nicotinamide ring must be positioned to transfer a hydride from C2 of isocitrate to the A-side of the ring. Nonetheless, model building of this complex is made difficult by the conformational flexibility of the $NADP^+$ molecule, the low affinity of the enzyme–$NADP^+$ interaction, and the remaining uncertainty about the nicotinamide conformation in the complex with the *E. coli* enzyme. The most plausible hypothesis places the nicotinamide in the anti conformation with the amide pointing toward serine 310 and aspartate 311 into the active site pocket, above isocitrate in the view shown in Figure 2. In an alternative hypothesis, the nicotinamide group binds in the syn conformation and the amide points toward lysine 100 and glutamate 336, to the left of isocitrate in the view shown in Figure 2. Most residues in both of these pockets are not conserved with IMDH, a further limitation on detailed model building. Although the hypothetical ternary complexes are subject to substantial uncertainties outlined above, the two possibilities are directly testable by site-directed mutagenesis of residues in the 310–311 region and 100 and 336 region, respectively. The crystallographic structures of binary substrate and cofactor complexes thus provide the foundation required for studies leading to a more complete understanding of the mechanism of $NADP^+$-dependent isocitrate dehydrogenase.

## Added in Proof

Haselbeck and McAlister-Henn (1991) have recently sequenced the $NADP^+$-dependent IDH of *Saccharomyces cerevisiae*. We have aligned the *E. coli* and *S. cerevisiae* sequences and found all isocitrate-binding site residues, except serine 113, are conserved between the two enzymes. This supports the comparison of the *E. coli* IDH structure with kinetic and spectroscopic results obtained for the eukaryotic enzyme.

## Acknowledgments

We thank Joseph Villafranca, Roberta Colman, and Jim Remington for helpful discussions, and the anonymous reviewers of *Biochemistry* for their comments on an earlier version of this paper.

**Registry No.** NADP-IDH, 9028-48-2; $NADP^+$, 53-59-8; Asp, 56-84-8; Mg, 7439-95-4; magnesium isocitrate, 23095-92-3.

## References

Adams, M. J., Ford, G. C., Koekok, R., Lentz, P. J., Jr., McPherson, A., Jr., Rossmann, M. G., Smiley, I. E., Schevitz, R. W., & Wonacott, A. J. (1970) *Nature 227*, 1098–1103.

Adams, M. J., Archibald, I. G., Bugg, C. E., Carne, A., Gover, S., Helliwell, J. R., Pickersgill, R. W., & White, S. W. (1986) *EMBO J. 2*, 1009–1014.

Bagchi, S., Wise, L. S., Brown, M. L., Bregman, D., Sul, H. S., & Rubin, C. S. (1987) *J. Biol. Chem. 262*, 1558–1565.

Branden, C.-I., Jornvall, H., Eklund, H., & Furugren, B. (1975) in *The Enzymes* (Boyer, P. D., Ed.) 3rd ed., Vol. 11, pp 104–190, Academic, New York.

Brooks, B. R., Bruccoleri, R. E., Olafson, B. D., States, D. J., Swaminathan, S., & Karplus, M. (1983) *J. Comput. Chem. 4*, 187–217.

Brunger, A. T., Kuriyan, K., & Karplus, M. (1987) *Science 235*, 458–460.

Clarke, A. R., Wigley, D. B., Chia, W. N., Barstow, D., Atkinson, T., & Holbrook, J. J. (1986) *Nature 324*, 699–702.

Dean, A. M., & Koshland, D. E., Jr. (1990) *Science 249*, 1044–1046.

Dean, A. M., Lee, M. H. I., & Koshland, D. E., Jr. (1989) *J. Biol. Chem. 264*, 20482–20486.

Ehrlich, R. S., & Colman, R. F. (1985) *Biochemistry 24*, 5378–5387.

Ehrlich, R. S., & Colman, R. F. (1987) *Biochemistry 26*, 2461–3471.

Ehrlich, R. S., & Colman, R. F. (1989) *Biochemistry 28*, 2058–2065.

Fita, I., & Rossmann, M. G. (1985) *Proc. Natl. Acad. Sci. U.S.A. 82*, 1604–1608.

Gandour, R. D. (1981) *Bioorg. Chem. 10*, 169–176.

Grissom, C. B., & Cleland, W. W. (1988) *Biochemistry 27*, 2934–2943.

Haselbeck, R. J., & McAlister-Henn, L. (1991) *J. Biol. Chem. 266*, 2339–2345.

Howard, A. J., Gilliland, G. L., Finzel, B. C., Poulos, T. L., Ohlendorf, D. H., & Salemme, F. R. (1987) *J. Appl. Crystallogr. 20*, 383–387.

Hurley, J. H., Thorsness, P. E., Ramalingam, V., Helmers, N. H., Koshland, D. E., Jr., & Stroud, R. M. (1989) *Proc. Natl. Acad. Sci. U.S.A. 86*, 8635–8639.

Hurley, J. H., Dean, A. M., Sohl, J. L., Koshland, D. E., Jr., & Stroud, R. M. (1990) *Science 249*, 1012–1016.

Kakinuma, K., Ozawa, K., Fujimoto, Y., Akutsu, N., & Oshima, T. (1989) *J. Chem. Soc., Chem. Commun.*, 1190–1192.

Kagawa, Y., Nojima, H., Nukiwa, N., Ishizuka, M., Nakajima, T., Yasuhara, T., Tanaka, T., & Oshima, T. (1984) *J. Biol. Chem. 259*, 2956-2960.
Kim, J.-J. P., & Wu, J. (1988) *Proc. Natl. Acad. Sci. U.S.A. 85*, 6677-6681.
Kobayashi, K., Doi, S., Negoro, S., Urabe, I., & Okada, H. (1989) *J. Biol. Chem. 264*, 3200-3205.
Jones, T. A. (1985) *Methods Enzymol. 115*, 157-170.
Lienhard, G. E., & Rose, I. A. (1964) *Biochemistry 3*, 185-190.
Londesborough, J. C., & Dalziel, K. (1968) *Biochem. J. 110*, 223-230.
Mas, M. T., & Colman, R. F. (1985) *Biochemistry 24*, 1643-1646.
McKee, J. S., Hlodan, R., & Nimmo, H. G. (1989) *Biochimie 71*, 1059-1064.
Nakamoto, T., & Vennesland, B. (1960) *J. Biol. Chem. 235*, 202-204.
Oppenheimer, N. J. (1987) in *Pyridine Nucleotide Coenzyme: Chemical, Biochemical, and Medical Aspects* (Dolphin, D., Poulson, R., & Avramovic, O., Eds.) Vol. 2A, pp 323-365, John Wiley and Sons, New York.
Richardson, J. S. (1981) *Adv. Protein Chem. 34*, 167-339.
Rossmann, M. G., Moras, D., & Olsen, K. W. (1974) *Nature 250*, 194-199.
Saenger, W., Reddy, B. S., Muhlegger, K., & Weimann, G. (1977) *Nature 267*, 225-229.
Scrutton, N. S., Berry, A., & Perham, R. N. (1990) *Nature 343*, 38-43.
Seltzer, S., Hamilton, G. A., & Westheimer, F. H. (1959) *J. Am. Chem. Soc. 81*, 4018-4024.
Siebert, G., Carsiotis, M., & Plaut, G. W. E. (1957) *J. Biol. Chem. 226*, 977-991.
Steinberger, R., & Westheimer, F. H. (1951) *J. Am. Chem. Soc. 73*, 429-435.
Thorsness, P. E., & Koshland, D. E., Jr. (1987) *J. Biol. Chem. 262*, 10422-10425.
van der Helm, D., Glusker, J. P., Johnson, C. K., Minkin, J. A., Burow, N. E., & Patterson, A. L. (1968) *Acta Crystallogr. Sect. B 24*, 578-592.
Villafranca, J. J., & Colman, R. F. (1974) *Biochemistry 13*, 1152-1160.
Wierenga, R. K., De Maeyer, M. C. H., & Hol, W. G. J. (1985) *Biochemistry 24*, 1346-1357.

# Characterization of the 25-Kilodalton Subunit of the Energy-Transducing NADH-Ubiquinone Oxidoreductase of *Paracoccus denitrificans*: Sequence Similarity to the 24-Kilodalton Subunit of the Flavoprotein Fraction of Mammalian Complex I[†,‡]

Xuemin Xu, Akemi Matsuno-Yagi, and Takao Yagi*
*Division of Biochemistry, Department of Molecular and Experimental Medicine, The Scripps Research Institute, La Jolla, California 92037*

*Received April 23, 1991; Revised Manuscript Received June 14, 1991*

ABSTRACT: The NADH dehydrogenase complex isolated from *Paracoccus denitrificans* is composed of approximately 10 unlike polypeptides [Yagi, T. (1986) *Arch. Biochem. Biophys. 250*, 302-311]. Structural genes encoding the subunits of this enzyme complex constitute at least one gene cluster [Xu, X., Matsuno-Yagi, A., & Yagi, T. (1991) *Biochemistry 30*, 6422-6428]. The 25-kDa subunit (*NQO2*), which has been isolated from sodium dodecyl sulfate-polyacrylamide gels, is a polypeptide of this enzyme complex. The partial N-terminal amino acid sequence and amino acid composition of the *NQO2* subunit have been determined. On the basis of the amino acid sequence, the *NQO2* gene was found to be located 1.7 kilobase pairs upstream of the gene for NADH-binding subunit (*NQO1*). The complete nucleotide sequence of the *NQO2* gene was determined. It is composed of 717 base pairs and codes for 239 amino acid residues with a calculated molecular weight of 26 122. The *NQO2* subunit is homologous to the $M_r$ 24 000 subunit of the mammalian mitochondrial NADH-ubiquinone oxidoreductase which bears an electron paramagnetic resonance-visible binuclear iron-sulfur cluster (probably cluster N1b). Comparison of the predicted amino acid sequence of the *Paracoccus NQO2* subunit with those of its mammalian counterparts suggests putative binding sites for the iron-sulfur cluster. In addition, nucleotide sequencing shows the presence of two unidentified reading frames between the *NQO1* and *NQO2* genes. These are designated URF1 and URF2 and are composed of 261 and 642 base pairs, respectively. The possible function of the protein coded for the URF2 is discussed.

Aerobically grown *Paracoccus denitrificans* contains a mitochondrial-type respiratory chain (Stouthamer, 1980). The NADH-ubiquinone (UQ)[1] oxidoreductase of *P. denitrificans* is akin to its mitochondrial counterpart in terms of the presence

[†] This work was supported by U.S. Public Health Service Grants GM33712 to T.Y. and MO1 RR00833 to the General Clinical Research Center. This is Publication No. 6817-MEM from The Scripps Research Institute, La Jolla, CA.
[‡] The nucleic acid sequence in this paper has been submitted to GenBank under Accession Number J05337.
* To whom correspondence should be addressed.

[1] Abbreviations: UQ, ubiquinone; Q, quinone; complex I or NDH-1, energy-tranducing NADH-quinone oxidoreductase; complex III, ubiquinol-cytochrome *c* oxidoreductase; bp, base pair(s); FP, IP, and HP, flavoprotein, iron-sulfur protein, and hydrophobic protein fractions of complex I, respectively; SDS, sodium dodecyl sulfate; PVDF, poly(vinylidene difluoride); EPR, electron paramagnetic resonance; FeS cluster, iron-sulfur cluster; URF, unidentified reading frame; kDa, kilodalton(s).

0006-2960/91/0430-8678$02.50/0 